Compressive behavior and energy absorption of novel body-centered cubic lattice metamaterials incorporating simple cubic truss units

Xuehao Song [a], Chengjun Zeng [a,*], Junqi Hu [a], Wei Zhao [a,*], Liwu Liu [a], Yanju Liu [a,*], Jinsong Leng [b]

[a] *Department of Astronautical Science and Mechanics, Harbin Institute of Technology (HIT), No. 92 West Dazhi Street, PO Box 301, Harbin 150001, People's Republic of China*
[b] *Center for Composite Materials and Structures, Harbin Institute of Technology (HIT), No. 2 YiKuang Street, Harbin 150080, People's Republic of China*

ABSTRACT

To enhance the compressive performance and energy absorption capabilities of conventional body-centered cubic (BCC) lattice structures, this study introduces a novel body-centered cubic (NBCC) lattice metamaterial incorporating simple cubic (SC) truss units. The NBCC design aims to achieve superior load-bearing capacity and improved energy dissipation under compressive loading conditions. Theoretical models based on Euler-Bernoulli and Timoshenko beam theories were developed to predict the equivalent elastic modulus and Poisson's ratio of the NBCC lattice metamaterials. Comprehensive finite element simulations and compression tests were conducted to systematically evaluate the compressive behavior and energy absorption characteristics of the metamaterials. Key parameters, including the edge length and beam diameter of the SC truss units, were varied to assess their impact on the mechanical performance of the metamaterials. Results indicate that increasing edge length yields higher equivalent elastic modulus, while specific energy absorption exhibits a peak-valley pattern accompanied by a tendency for premature failure. Conversely, enlarging the beam diameter enhances both the elastic modulus and specific energy absorption, albeit with increased fluctuations in the stress–strain response. This study provides valuable insights for the design and optimization of lattice metamaterials for advanced engineering applications.

1. Introduction

Mechanical metamaterials have emerged as a fascinating research field, captivating scientists and engineers with their extraordinary properties that arise from carefully engineered microstructures rather than their constituent materials. Metamaterials represent a class of artificially engineered composite structures that exhibit extraordinary physical properties not readily observed in naturally occurring materials. These artificially designed materials exhibit unique characteristics, such as adjustable Poisson's ratio [1–4], exceptional specific stiffness [5–9], and extraordinary energy absorption capacity [10–14], which are not commonly found in natural materials. The ability to tailor the mechanical properties of metamaterials through the rational design of their microstructures has opened up new possibilities for creating materials with unprecedented functionalities [15–18]. This has led to a paradigm shift in materials science, where the focus has shifted from relying on the intrinsic properties of materials to exploiting the power of structural

design at the micro- and nanoscale [19–21].

The advent of mechanical metamaterials has opened up new avenues for innovative applications in various domains, including aerospace [22], automotive, and biomedical engineering [23], where lightweight, high-performance materials are highly sought. For instance, the development of lightweight, high-strength metamaterials could revolutionize the aerospace industry by enabling the design of more fuel-efficient aircraft with improved structural integrity [24]. Similarly, in the biomedical field, mechanical metamaterials with tailored properties could be used to create advanced implants and prosthetics that closely mimic the mechanical behavior of natural tissues [25]. The potential impact of mechanical metamaterials extends beyond these traditional domains, with promising applications in areas such as energy harvesting, vibration control, and acoustic manipulation [26–28].

Among the diverse classes of mechanical metamaterials, lattice metamaterials have garnered significant attention due to their remarkable combination of low density and superior mechanical properties

---

[29–35]. Lattice metamaterials are typically inspired by the crystalline lattice structures found in materials, such as face-centered cubic (FCC) [34], body-centered cubic (BCC) [36], simple cubic (SC), and hexagonal close-packed (HCP) lattices [37]. These periodic architectures are composed of a network of interconnected struts or beams, which collectively determine the overall mechanical behavior of the meta-material. By carefully designing the geometry and arrangement of these struts, it is possible to achieve a wide range of mechanical properties that are not attainable with conventional materials. These lattice met-amaterials can be broadly categorized into two types based on their deformation mechanisms: stretch-dominated and bending-dominated lattice metamaterials [34]. Stretch-dominated lattice metamaterials exhibit higher stiffness and strength compared to bending-dominated metamaterials, as the struts in the former primarily undergo axial deformation. This is because the stretching deformation mode requires more energy than the bending mode, leading to a higher resistance to deformation. On the other hand, bending-dominated lattice meta-materials are characterized by their ability to undergo large de-formations without significant increase in stress, making them ideal for applications that require high compliance and energy absorption.

Extensive research efforts have been dedicated to investigating the mechanical properties of lattice metamaterials, with a particular focus on their compressive behavior, bending performance, and impact resistance [38,39]. In terms of compressive behavior, lattice meta-materials have demonstrated remarkable energy absorption capabilities, making them ideal candidates for applications such as protective gear and impact mitigation. Li et al. employed machine learning methods to optimize the cubic lattice metamaterials, enabling the inverse design of metamaterials and the prediction of potential structures for extreme target properties beyond the training domain [40]. Logakannan et al. introduced a novel star-shaped lattice structure with cross-linking struts at the junctions, which exhibited a lower Poisson's ratio and higher elastic modulus compared to the non-cross-linked counterparts [41]. Nian et al. developed a bio-inspired functionally graded lattice-infilled protective structure, aimed at enhancing the energy absorption char-acteristics under ship impact loads [42].

Despite significant advancements, research on lattice metamaterials still faces challenges. For instance, the BCC and SC lattices, both widely studied and comprising eight struts each, exhibit distinct mechanical behaviors. The BCC lattice relies on a bending-dominated deformation mechanism, providing superior energy absorption but reduced compressive strength. In contrast, the SC lattice undergoes axial defor-mation, resulting in high compressive strength yet compromised energy absorption efficiency. Consequently, a primary challenge for researchers is to design a metamaterial that simultaneously achieves high energy absorption and robust compressive performance.

To overcome these challenges, we introduce a novel body-centered cubic (NBCC) lattice metamaterial that incorporates SC truss units. By strategically combining the beneficial characteristics of BCC and SC lattices through specific assembly methods, this design achieves enhanced load-bearing capabilities and improved energy absorption performance under compressive loading. Rather than necessitating entirely new structural configurations, this design methodology extends the design space of lattice metamaterials through strategic combination of existing structures that have demonstrated exceptional properties. This study develops theoretical models for NBCC units using Timo-shenko and Euler-Bernoulli beam theories to predict the effective elastic modulus and Poisson's ratio of NBCC lattice metamaterials. Finite element simulations and compression tests were performed, and the experimental data were compared with theoretical predictions to vali-date the models systematically. Additionally, the compression behavior and energy absorption characteristics of NBCC lattice metamaterials were analyzed to identify optimal geometric parameters.
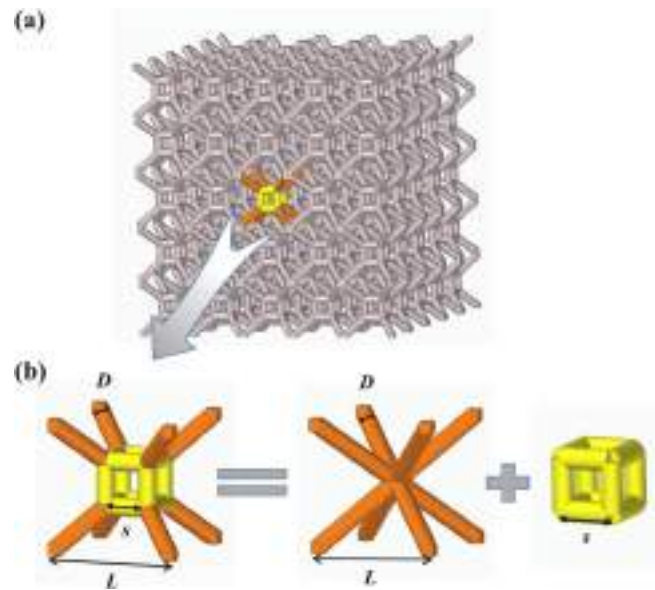

Fig. 1. Design of the NBCC lattice metamaterial. (a) Schematic illustration of the lattice metamaterial composed of an array of NBCC units. (b) Schematic representation of the NBCC unit.

2. Design of NBCC lattice metamaterials

The study presents a novel NBCC lattice metamaterial, as illustrated in Fig. 1a, which is composed of an array of NBCC units. Each NBCC unit is a combination of a conventional BCC truss unit and an SC truss unit, as shown in Fig. 1b. The edge length of the NBCC unit is denoted as L, while the edge length of the SC truss unit is represented by s. All beams within the structure have a uniform radius of D. To investigate the mechanical properties of NBCC lattice metamaterial, a load is applied in the vertical direction.

The primary distinction between Euler-Bernoulli beam theory and Timoshenko beam theory lies in their treatment of shear deformation effects. Euler-Bernoulli beam theory is founded on two fundamental assumptions: 1) The cross-sections that are perpendicular to the neutral axis before deformation remain planar after deformation. 2) The cross-sections remain perpendicular to the beam axis after deformation. In contrast, Timoshenko beam theory retains the first assumption but ac-counts for shear deformation, resulting in additional deflection and causing the cross-sections to no longer be perpendicular to the beam axis (Fig. 2). When the shear modulus of the beam material approaches in-finity, the beam behaves as a shear-rigid body, and Timoshenko beam theory converges to Euler-Bernoulli beam theory in the absence of rotational inertia considerations. Timoshenko beam theory employs a linear distribution assumption for the displacement field, categorizing it as a first-order shear deformation theory. Although higher-order shear deformation theories can more accurately approximate actual behavior through nonlinear displacement distributions, they impose more strin-gent boundary conditions and entail greater computational complexity. To balance computational efficiency and accuracy, this study employs both Timoshenko and Euler-Bernoulli beam theories.

When analyzing the deformation of an NBCC unit (Fig. 3a) with an internal cube edge length of s and an effective strut length of l', the deformation is primarily associated with struts ① and ② (Fig. 3b). The force F is divided into $F_1 = Fcos\theta$, $F_2 = Fsin\theta$ in the plane shown in Fig. 3b, where θ is angle between beam and vertical direction. The deformation of these struts is examined using both Euler-Bernoulli and Timoshenko beam theories.

Firstly, considering Euler-Bernoulli beam theory, the analysis of strut ① is identical to that of the BCC unit (see Supporting Information). The axial displacement and the deflection perpendicular to the axial
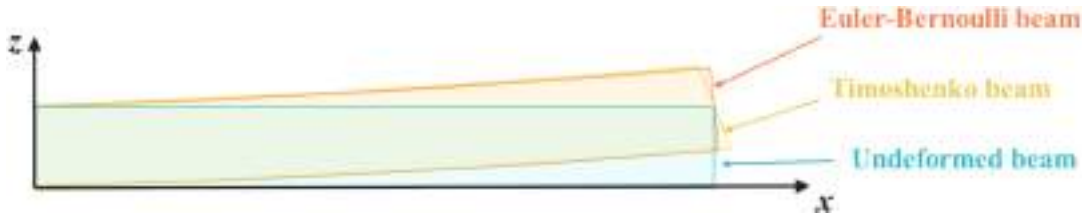
Fig. 2. Comparison of the cross-sections perpendicular to the neutral axis after deformation in Euler-Bernoulli and Timoshenko beam theories.
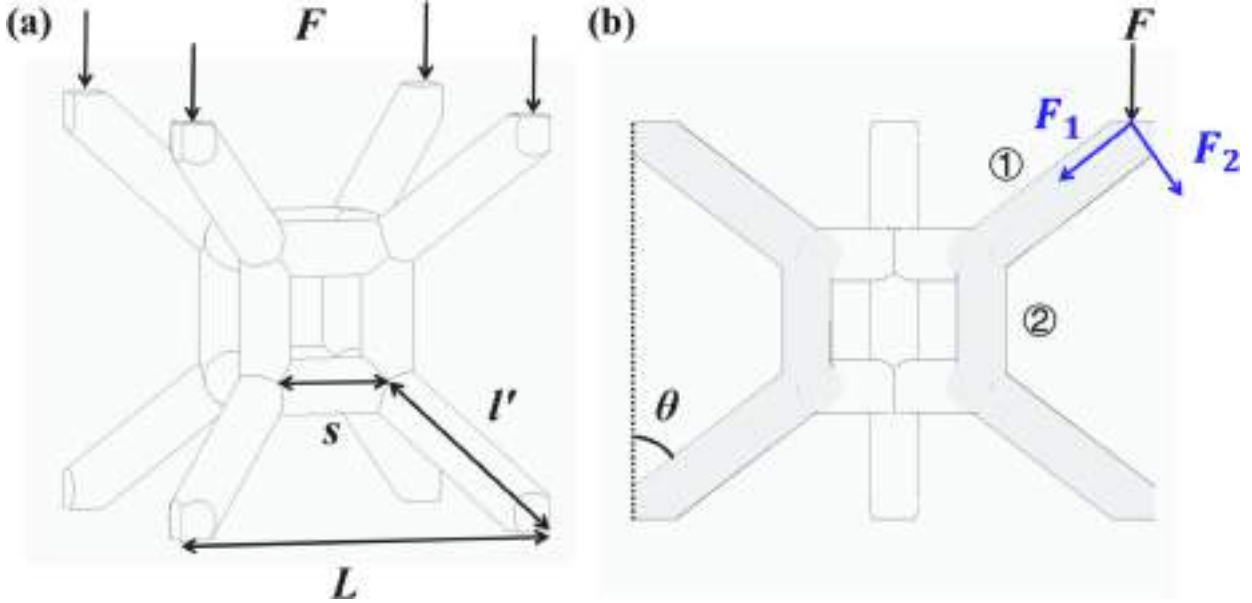

Fig. 3. Schematic representation of the force distribution in an NBCC unit under compressive loading. (a) 3D illustration. (b) Cross-sectional view along the diagonal.

direction are expressed as follows

$$\delta_{F_1} = \frac{F_1 l'}{E_0 A} \tag{1}$$

$$\delta_{F_2} = \frac{F_2 l'^3}{3E_0 I} \tag{2}$$

where $A = \frac{\pi D^2}{4}$, $I = \frac{\pi D^4}{64}$, $l' = \frac{\sqrt{3}(L-s)}{2}$, E_0 is the Young's modulus of the raw material.

For strut ②, according to the force translation theorem, it is subjected to a vertically downward force and an additional torque due to the translated force. As the struts in the SC lattice unit are relatively short and the horizontal struts bear a portion of the torque, the influence of the torque is neglected in this analysis, and only the vertically downward force F is considered. Consequently, the deformation of strut ② is given by

$$\delta_N = \frac{Fs}{2E_0 A} \tag{3}$$

Analyzing the deformation using Timoshenko beam theory, the approach remains the same, yielding the corresponding deformations

$$\delta_{F_1} = \frac{F_1 l'}{E_0 A} \tag{4}$$

$$\delta_{F_2} = \frac{F_2 l'^3}{12E_0 I}\left(1 + \frac{12E_0 I}{\kappa A G_0 l'^2}\right) \tag{5}$$

$$\delta_N = \frac{Fs}{2E_0 A} \tag{6}$$

For cylindrical beam, $\kappa = \frac{6(1+\mu)^2}{7+12\mu+4\mu^2}$, where κ is Timoshenko shear coefficient [43] and μ is the Poisson's ratio of the material. For isotropic materials, $G_0 = \frac{E_0}{2(1+\mu)}$.

Thus, Eq. (5) can be expressed as

$$\delta_{F_2} = \frac{kF_2 l'^3}{12E_0 I} \tag{7}$$

where k is defined to comprehensively represent the coupling effect of bending and shear, $k = 1 + \frac{7+12\mu+4\mu^2}{1+\mu}\left[\frac{D}{\sqrt{3}(L-s)}\right]^2$

Based on the geometric relationships, the displacements of the NBCC along each direction can be derived as follows

$$u = v = \frac{1}{\sqrt{2}}(\delta_{F_2}cos\theta - \delta_{F_1}sin\theta) \tag{8}$$

$$w = -(\delta_{F_2}sin\theta + \delta_{F_1}cos\theta + 2\delta_N) \tag{9}$$

Under compressive loading conditions, the equivalent elastic modulus of the NBCC is given by

$$E_s = \frac{\sigma_z}{\varepsilon_z} = \frac{-\frac{4F}{L^2}}{\frac{w}{L}} = -\frac{4F}{wL} \tag{10}$$

The equivalent Poisson's ratio of the NBCC is expressed as

$$\mu_s = -\frac{2u}{w} \tag{11}$$

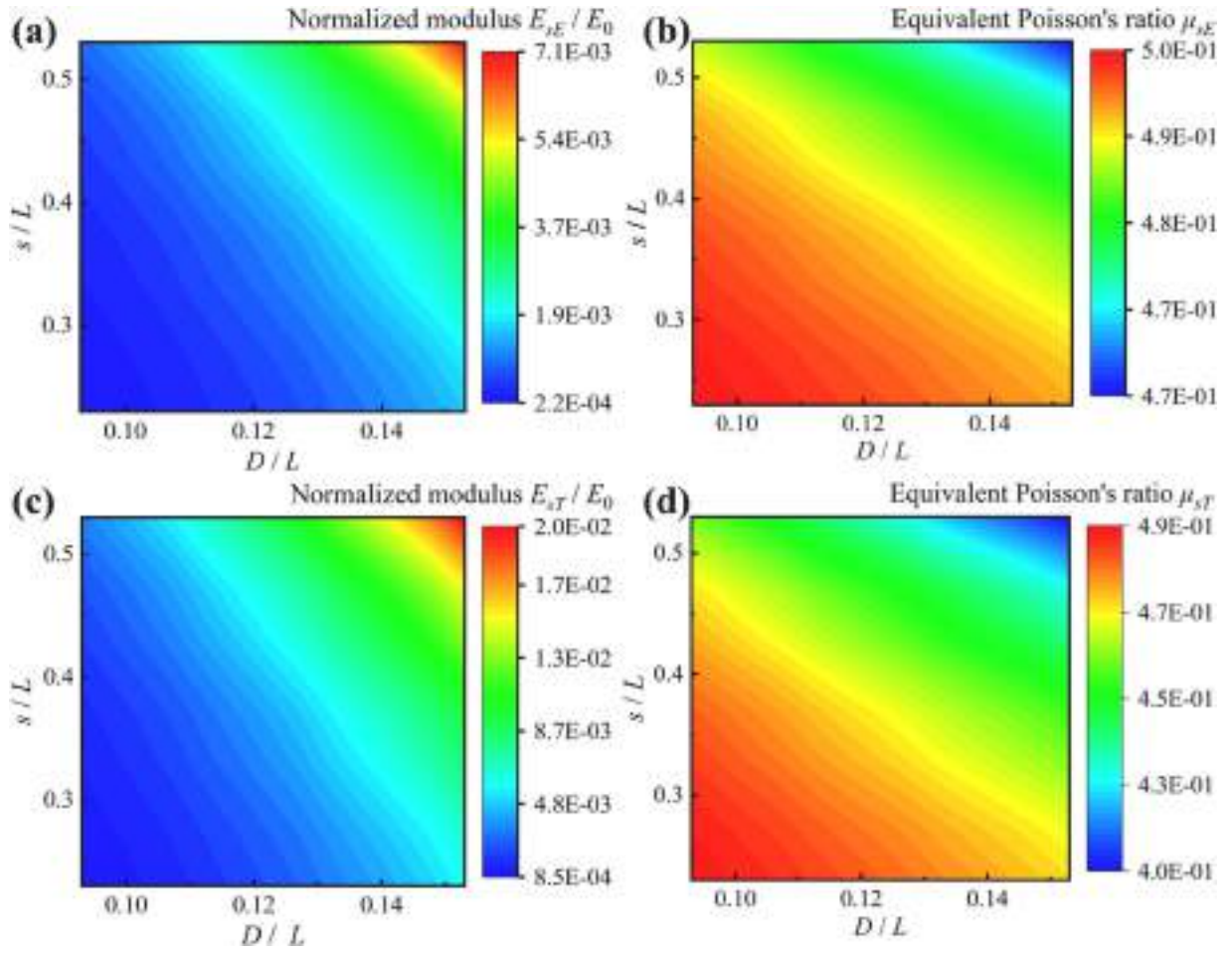Substituting Eq. (8)–(9) into Eq. (10)–(11) yields the effective elastic

Fig. 4. The normalized elastic modulus and equivalent Poisson's ratio based on Euler-Bernoulli beam theory and Timoshenko beam theory. (a) Normalized elastic modulus and (b) equivalent Poisson's ratio of NBCC lattice metamaterial versus dimensionless parameters s / L and D / L, obtained using the Euler-Bernoulli beam theory. (c) Normalized elastic modulus and (d) equivalent Poisson's ratio of NBCC lattice metamaterial as a function of dimensionless parameters s / L and D / L, derived from the Timoshenko beam theory.

modulus and Poisson's ratio of the NBCC.

1. Equivalent elastic modulus and Poisson's ratio of NBCC based on Euler-Bernoulli beam theory:

$$E_{sE} = \frac{2\sqrt{3}E_0\pi D^4}{L\left[8(L-s)^3 + (L+s)D^2\right]} \tag{12}$$

$$\mu_{sE} = \frac{4(L-s)^3 - (L-s)D^2}{8(L-s)^3 + (L-s)D^2 + 2\sqrt{3}sD^2} \tag{13}$$

2. Equivalent elastic modulus and Poisson's ratio of NBCC based on Timoshenko beam theory:

$$E_{sT} = \frac{2\sqrt{3}E_0\pi D^4}{L\left[2k(L-s)^3 + (L+s)D^2\right]} \tag{14}$$

$$\mu_{sT} = \frac{k(L-s)^3 - (L-s)D^2}{2k(L-s)^3 + (L-s)D^2 + 2\sqrt{3}sD^2} \tag{15}$$

Fig. 4 presents the variations in normalized elastic modulus and effective Poisson's ratio of the NBCC lattice metamaterial as functions of dimensionless parameters s / L and D / L, obtained using the proposed theoretical approach. The results are derived from both the Euler-Bernoulli and Timoshenko beam theories, providing a comprehensive understanding of the metamaterial's mechanical properties and their dependence on the geometric parameters of the lattice structure. The Euler-Bernoulli beam theory is used to obtain the normalized elastic modulus (Fig. 4a) and equivalent Poisson's ratio (Fig. 4b), while the Timoshenko beam theory is employed to derive the normalized elastic modulus (Fig. 4c) and equivalent Poisson's ratio (Fig. 4d). The comparison between the two theories offers insights into the accuracy and limitations of each approach in predicting the mechanical behavior of the NBCC lattice metamaterial.

3. Materials and methods

3.1. Sample fabrication

The equivalent elastic modulus of NBCC lattice metamaterials, as shown in Eq. (12) and (14), depends solely on the edge length L of the NBCC unit, the edge length s of the SC truss unit, and the diameter D of the beams. This study primarily investigates the influence of s and D on the compressive performance and energy absorption capacity of NBCC lattice metamaterials, while keeping L constant. All metamaterials are constructed by arranging the corresponding NBCC units in a three-axial array consisting of 27 units. The edge length L is set to 15 mm, and four different edge lengths of the SC truss unit s ($s = 4, 5, 6,$ and 7 mm) and three beam diameters D ($D = 1.6, 1.8, 2.0$ mm) are considered. The
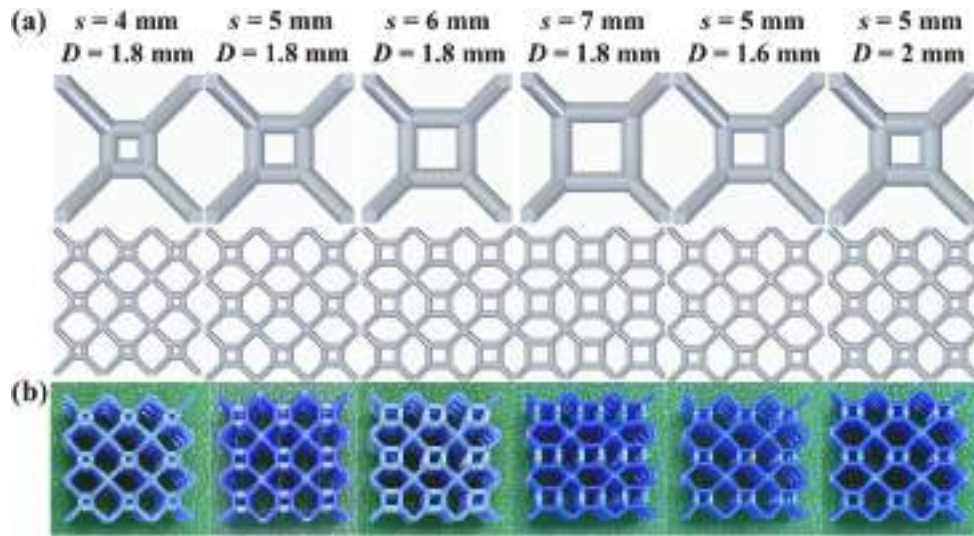
Fig. 5. Design and fabrication of NBCC lattice metamaterials. (a) Designed metamaterial models with different parameter combinations. (b) Metamaterial samples fabricated via 3D printing.
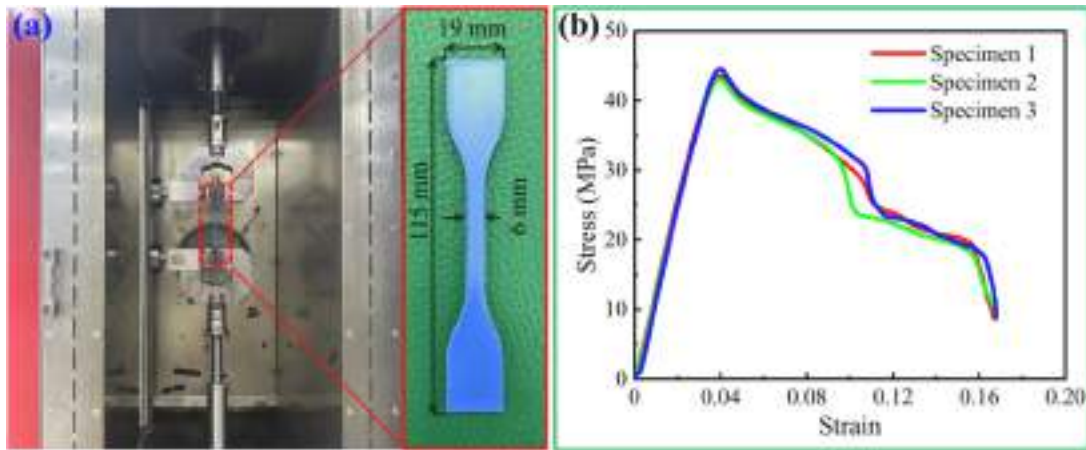

Fig. 6. Tensile testing of PLA specimens. (a) Photograph of the specimens and testing apparatus. (b) Measured true stress–strain curves.

designed NBCC lattice metamaterial models are illustrated in Fig. 5a.

In this study, NBCC lattice metamaterial samples were fabricated using 3D printing technology. A fused deposition modeling (FDM) 3D printer (Anycubic Mega-S) was utilized, and polylactic acid (PLA) filament served as the printing material. To balance printing efficiency and accuracy, a moderate printing speed of 40 mm/s was selected. The PLA filament has a melting temperature of approximately 170 °C. Therefore, the nozzle temperature was set slightly higher at 210 °C. The nozzle diameter was maintained at 0.4 mm, and the platform temperature was kept at 50 °C. The prepared samples are shown in Fig. 5b.

3.2. Experimental methods

3.2.1. Tensile test of standard samples

To obtain the material parameters of the PLA, including Young's modulus and elastoplastic parameters, dumbbell-shaped tensile specimens with a thickness of 2 mm were fabricated by 3D printing, following the ASTM standard D638. A printing orientation of $\pm 45°$ was selected to provide approximate values for assessing the material properties of the 3D printed PLA. Quasi-static tensile tests of the PLA specimens were conducted at room temperature (approximately 25 °C) using a Zwick/Roell Z10 electronic universal testing machine (Fig. 6a). The gauge length and loading rate were set to 45 mm and 2 mm/min, respectively.

The obtained true stress–strain curves of the PLA specimens are presented in Fig. 6b. The linear segment of the curves was used to determine the Young's modulus of PLA, which was found to be $E_0 = 1261$ MPa.

3.2.2. Compression tests of NBCC lattice metamaterials

To evaluate the compressive performance and energy absorption capability of the designed NBCC lattice metamaterials, compression tests were conducted on the metamaterial samples. The compression tests were performed on a Zwick/Roell Z50 electronic universal testing machine following ASTM standard D1621. A low loading rate of 4 mm/min was adopted to simulate the quasi-static loading process. During loading, load–displacement data were collected in real-time, and the compression deformation of the metamaterial samples was recorded using a digital camera. For each type of sample, three identical tests were carried out to ensure data reproducibility. As the metamaterial samples exhibited relative sliding phenomena when compressed to a certain extent, the strain range used for calculating the energy absorption (EA) was determined using the EA efficiency method [44]. The EA efficiency η is defined as the ratio of the area enclosed by the equivalent stress–strain curve of the metamaterial and the strain axis to the instantaneous stress, i.e.,

Table 1
The plastic parameters of the raw material determined from the tensile stress–strain curve of PLA.

Stress / MPa	20.03	31.52	40.93	42.04	43.98	35.77	27.56	20.04
Plastic Strain	0	0.008	0.018	0.019	0.022	0.060	0.083	0.125
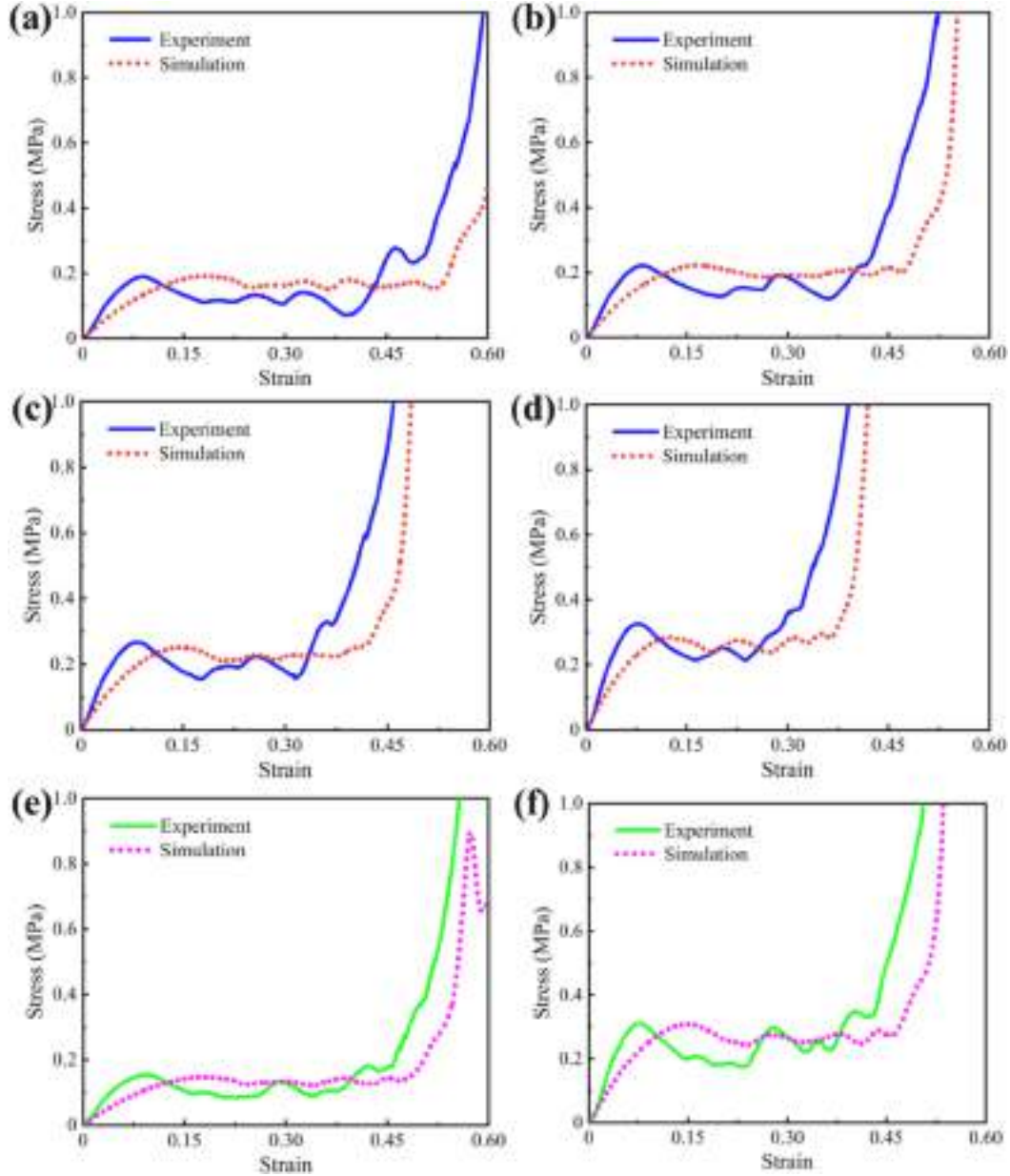
Fig. 7. Equivalent stress–strain curves of NBCC lattice metamaterials with various geometric parameters obtained from experiments and finite element simulations. (a) $s = 4$ mm, $D = 1.8$ mm. (b) $s = 5$ mm, $D = 1.8$ mm. (c) $s = 6$ mm, $D = 1.8$ mm. (d) $s = 7$ mm, $D = 1.8$ mm. (e) $s = 5$ mm, $D = 1.6$ mm. (f) $s = 5$ mm, $D = 2.0$ mm.

$$\eta = \frac{\int_0^\varepsilon \sigma(\varepsilon)d\varepsilon}{\sigma(\varepsilon)} \tag{16}$$

The densification strain ε_d is defined as the strain at which the EA efficiency reaches its maximum value and can be calculated using the following equation

$$\frac{d\eta(\varepsilon)}{d\varepsilon}\bigg|_{\varepsilon=\varepsilon_d} = 0 \tag{17}$$

3.3. Finite element simulations

Finite element simulations were performed using the commercial software ABAQUS/EXPLICIT 2023 to investigate the compression deformation mechanisms of the NBCC lattice metamaterials. 3D finite element models were created based on the geometric designs of the metamaterials. Four-node linear tetrahedral elements (C3D4) were used in all finite element models to balance computational accuracy and efficiency. Discrete rigid planar plates were created at the top and bottom of the metamaterial models to incorporate boundary conditions similar to those in the compression experiments, where all degrees of freedom of

the bottom rigid plate were constrained, while the top rigid plate underwent a uniform vertical displacement. General contact was employed to simulate the interactions between different parts of the model. A "hard" contact with tangential frictional behavior was defined for the entire model, and the tangential friction coefficient was set to 0.2. Mesh convergence analysis was performed to obtain a suitable mesh size, which was ultimately determined to be 0.35 mm. Since PLA exhibits typical viscoplastic mechanical behavior, an isotropic plasticity model was adopted to define its material properties in the finite element simulation. The plastic parameters of the raw material were obtained from the tensile stress–strain curve of PLA shown in Fig. 6b and are presented in Table 1. Other required input material parameters include a density of 1250 kg/m^3, Young's modulus of 1261 MPa, and Poisson's ratio of 0.4.

4. Results and discussion

4.1. Equivalent stress–strain curves

Fig. 7 shows the equivalent stress–strain curves for NBCC lattice metamaterials with different geometric parameters, obtained from experiments and finite element simulations. All curves go through three stages: first, an initial elastic stage where stress increases linearly with strain, indicating high stiffness. Next is the plateau stage, where stress stays nearly constant or rises slowly as the lattice structure collapses and deforms plastically, allowing significant energy absorption. Finally, in the densification stage, stress rises sharply due to increased interactions between the deformed lattice struts and the reduction of voids in the structure. The close match between the experimental and simulated curves shows that the finite element modeling accurately captures the mechanical behavior of NBCC lattice metamaterials with various geometries.

Fig. 7a-7d reveals that as the edge length *s* of the SC truss unit increases, the equivalent elastic modulus of the NBCC lattice metamaterials also increases. The finite element simulation curves exhibit a longer plateau stage than the experimental curves, which can be attributed to the more uniform deformation of the struts dominated by bending under ideal conditions. Experimental observations from Fig. 7c and 7d demonstrate that metamaterials with relatively large edge lengths *s* tend to enter the densification stage prematurely during compression. This phenomenon can be attributed to early-onset instability and structural buckling during loading, caused by increased axial beam length, ultimately leading to global structural displacement. On the other hand, when the edge length *s* remains constant while the beam diameter *D* is increased, a significant enhancement in the compressive performance is observed, as shown in Fig. 7b, 7e, and 7f. However, metamaterials with larger strut diameters *D* exhibit more pronounced stress fluctuations, attributed to layer-wise failure mechanisms, resulting in abrupt stress variations. These findings highlight the complex interplay between the geometric parameters of the SC truss unit and the mechanical behavior of the NBCC lattice metamaterials, providing valuable insights for the design and optimization of these advanced materials for various engineering applications.

4.2. Equivalent elastic modulus and energy absorption

Section 2 shows that analytical expressions alone cannot determine whether Euler-Bernoulli or Timoshenko beam theory better matches the experimental elastic constants of NBCC lattice metamaterials. However, if the material's Poisson's ratio is known, adjusting the radius-to-length ratio of the cylindrical struts can make the elastic constants from both theories identical when *k* is four. Since common materials have Poisson's ratios between 0.2 and 0.5, setting *k* to four indicates that the struts are short and thick. Therefore, for short and thick struts, there is no significant difference between the equivalent elastic constants derived from Euler-Bernoulli and Timoshenko beam theories.
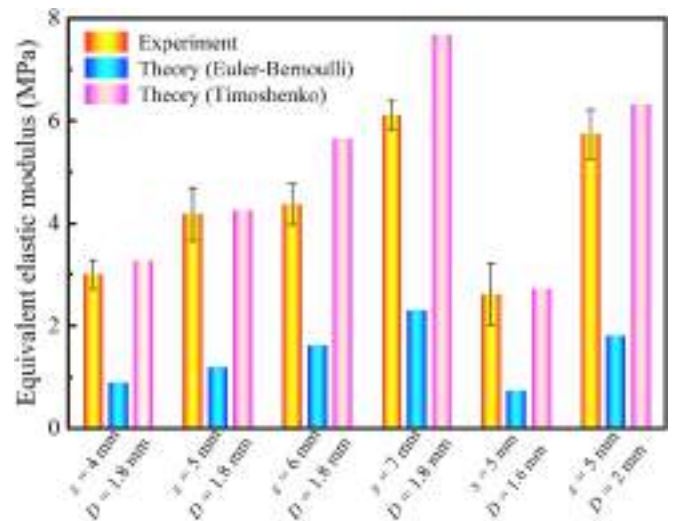

Fig. 8. Comparison of the equivalent elastic modulus of NBCC lattice metamaterials obtained through experimental measurements and theoretical predictions based on Euler-Bernoulli beam and Timoshenko beam theories.

By substituting the Young's modulus E_0 of the raw material and the geometric parameters of the NBCC lattice metamaterial into Eq. (12) and (14), the equivalent elastic modulus of the metamaterial derived from Euler-Bernoulli beam and Timoshenko beam theories can be calculated, respectively. Fig. 8 presents a comparison of the equivalent elastic modulus of the NBCC lattice metamaterial obtained through experiments and theoretical calculations. It is evident that the equivalent elastic modulus based on Euler-Bernoulli beam theory is significantly smaller than that measured experimentally, while the equivalent elastic modulus based on Timoshenko beam theory shows good agreement with the experimental results. The reason for this discrepancy lies in the fact that the struts designed in the NBCC lattice metamaterials in this study are slender beams. Neglecting the influence of shear deformation leads to substantial errors when using the Euler-Bernoulli beam theory. These findings emphasize the necessity of accounting for shear deformation effects when analyzing and predicting the mechanical properties of NBCC lattice metamaterials with slender beams. Furthermore, they demonstrate that Timoshenko beam theory provides superior accuracy in capturing the equivalent elastic behavior of these advanced materials.

Based on the equivalent stress–strain curves of different metamaterials shown in Fig. 7, the corresponding densification strain (ε_d) for each metamaterial was determined using Eq. (16) and (17). Table S1 (Supporting Information) presents the calculated results of the densification strain for each metamaterial.

The specific energy absorption (SEA) of lattice metamaterials and other lightweight structures is a measure of the energy absorbed per unit mass during the compression process. The SEA is a key parameter that characterizes the energy absorption efficiency of these materials and is expressed as follows

$$\text{SEA} = \frac{\int_0^{\varepsilon d} \sigma(\varepsilon) d\varepsilon}{\rho^*} \tag{18}$$

where $\rho^* = \frac{\rho_0 V_b}{V}$ represents the effective density of the metamaterial, ρ_0 is material density, $V_b = \pi D^2 (\sqrt{3}L - \sqrt{3}s + 2s)$ represents total volume of all beams of the structure, $V = L^2$ represents cube space volume occupied by structure.

Table S2 (Supporting Information) presents the energy absorption values for structures with different geometric parameters before densification. The SEA of NBCC lattice metamaterials with varying parameters was calculated using both experimental data and finite element simulations, as depicted in Fig. 9.
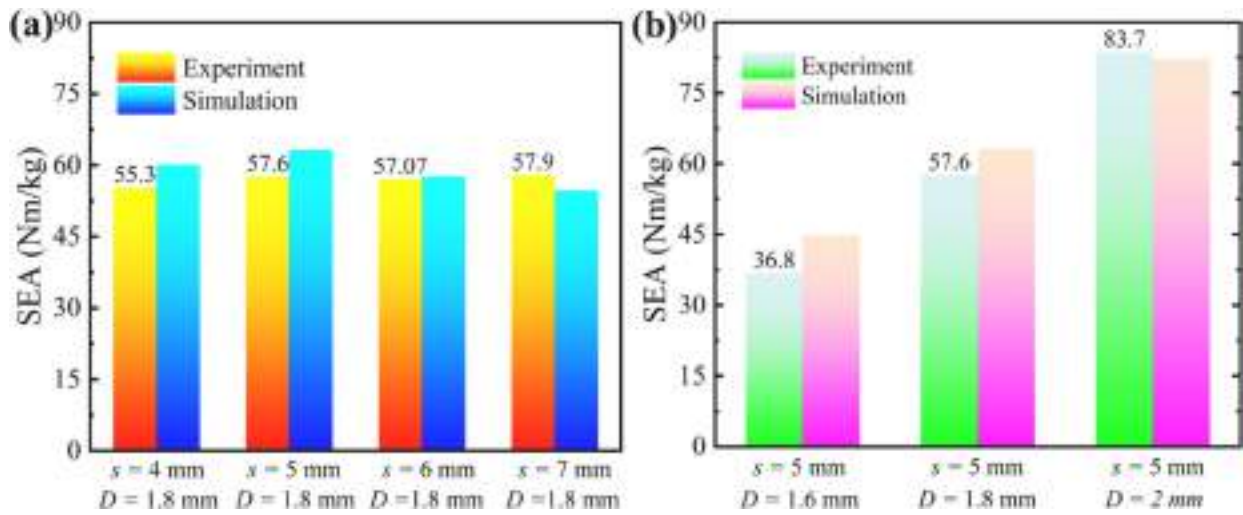
Fig. 9. SEA of NBCC lattice metamaterials with varying parameters. (a) Constant *D* and varying *s*. (b) Constant *s* and varying *D*.
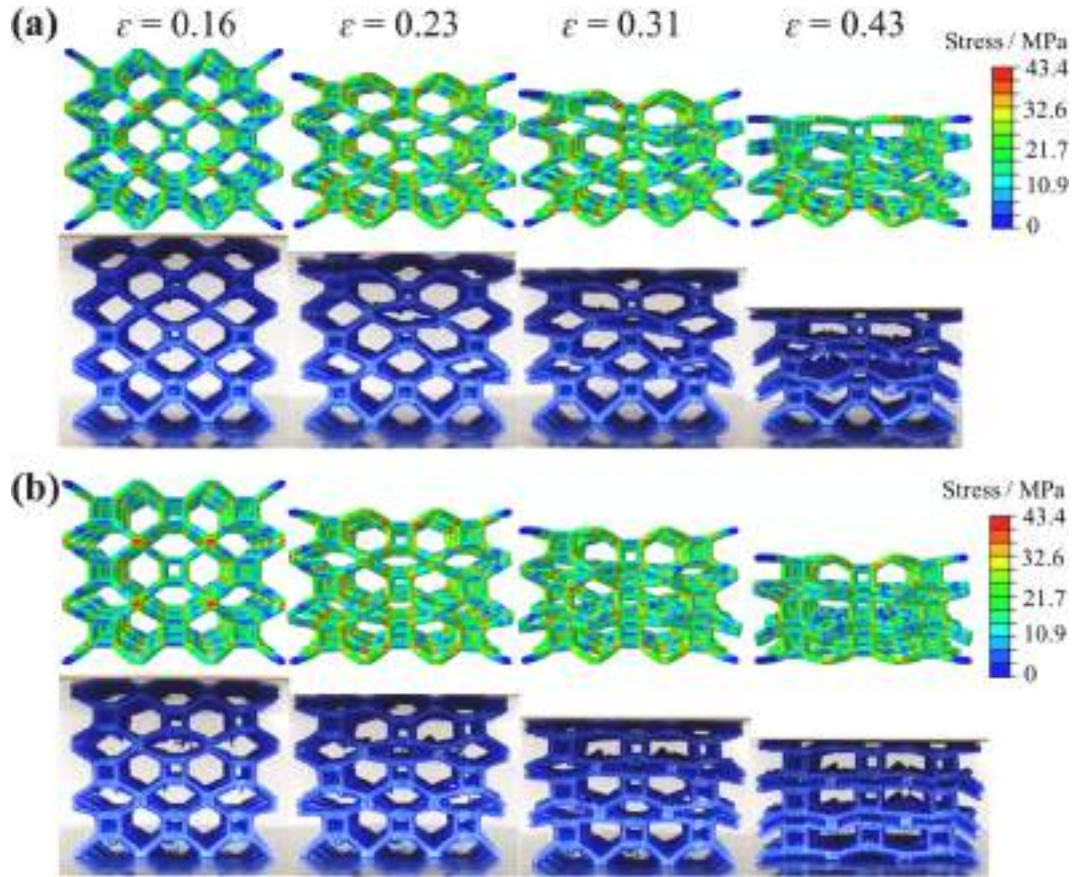

Fig. 10. Compressive deformation process of NBCC lattice metamaterials with constant *D* and varying *s*, obtained through finite element simulations and experiments. (a) *s* = 4 mm, *D* = 1.8 mm. (b) *s* = 5 mm, *D* = 1.8 mm.

As illustrated in Fig. 9, the SEA of NBCC lattice metamaterials exhibits a clear dependence on the geometric parameters of the SC truss unit. When *s* is fixed at 5 mm, SEA increases as the beam diameter *D* increases. When *D* is fixed at 1.8 mm, SEA initially rises and then declines with increasing *s*, reaching its maximum at *s* = 5 mm. This behavior is attributed to the effective density rising with both *s* and *D*. Larger *D* values enhance the structure's resistance to shear deformation and improve its load-bearing capacity, resulting in an energy absorption rate that exceeds the rate of density increase, thereby elevating SEA.

Additionally, as *s* increases, the structure more readily enters the densification stage while simultaneously enhancing its load-bearing capacity. According to the data presented in Table S2 (Supporting Information), the combined effects of these factors cause an initial increase followed by a subsequent decrease in energy absorption, leading to the observed peak-valley pattern in SEA values. This trend suggests that the beam diameter plays a crucial role in determining the energy absorption capacity of the NBCC lattice metamaterials, with larger diameters resulting in higher SEA. Notably, the SEA obtained through finite
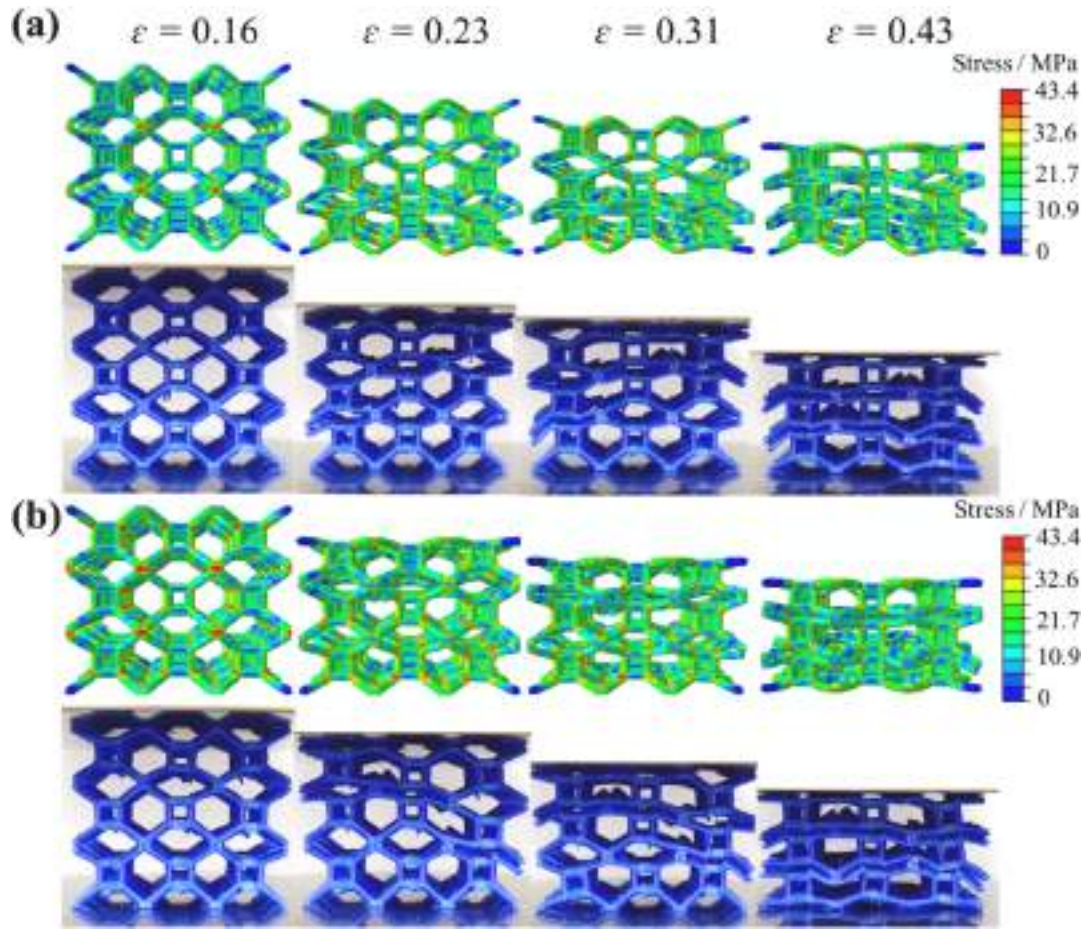
Fig. 11. Compressive deformation process of NBCC lattice metamaterials with constant *s* and varying *D*, obtained through finite element simulations and experiments. (a) *s* = 5 mm, *D* = 1.6 mm. (b) *s* = 5 mm, *D* = 2.0 mm.

element simulations is in good agreement with the experimental results, validating the numerical approach employed in this study.

4.3. Compression deformation mode

Fig. 10 and Fig. S2 (Supporting Information) present a comprehensive comparison of the compressive deformation process of NBCC lattice metamaterials with constant beam diameter *D* and varying edge length *s*, obtained through both finite element simulations and experimental observations. The failure mode of NBCC lattice metamaterials is characterized by a layer-by-layer collapse, where the top layer undergoes deformation first, initiated by the bending-dominated struts. As the effective strain increases, the bending-dominated struts experience extensive contact, leading to a significant load redistribution within the structure. At this stage, the stretch-dominated struts begin to play a crucial role in load-bearing, marking the onset of the plateau evolution stage of the metamaterial. The experimental results and finite element simulations accurately capture this progressive failure mechanism, showcasing the localized deformation and the transition from bending-dominated to stretch-dominated behavior.

Fig. 11 illustrates a detailed comparison of the compressive deformation patterns of NBCC lattice metamaterials with constant *s* and varying beam diameter *D*. The analysis reveals that struts with smaller diameters are more susceptible to premature failure at the connection points due to stress concentrations. This localized failure hinders the uniform and effective load transfer to the lower layers of the structure, compromising the overall mechanical performance of the metamaterial. The finite element simulations accurately capture this phenomenon, highlighting the critical role of beam diameter in the deformation and

failure mechanisms of NBCC lattice metamaterials. The experimental results corroborate the numerical findings, demonstrating the vulnerability of smaller-diameter struts to early failure and the consequent disruption of load distribution within the lattice structure.

5. Conclusions

In this study, a novel NBCC lattice metamaterial incorporating SC truss units is proposed to enhance the compressive load-bearing capacity and energy absorption performance of conventional BCC lattices. Theoretical prediction models for the effective elastic modulus and Poisson's ratio of NBCC lattice metamaterials are established based on Euler-Bernoulli and Timoshenko beam theories. The influence of SC truss unit parameters, such as edge length *s* and beam diameter *D*, on the compressive properties and energy absorption capability of NBCC lattice metamaterials is systematically investigated through compression experiments and finite element simulations. The results demonstrate that increasing *s* leads to higher effective elastic modulus of the metamaterial, while SEA exhibits a peak-valley pattern with its maximum value at *s* = 5 mm. The structure exhibits layer-by-layer collapse behavior, characterized by extensive contact between bending-dominated struts under increasing effective strain, leading to substantial internal load redistribution. Increasing *D* substantially enhances both the effective elastic modulus and SEA of the metamaterial. However, it also amplifies fluctuations in the plateau region of the stress–strain curve. The propensity for premature failure at connection points is heightened in struts of smaller diameter, owing to stress concentration. This localized failure compromises uniform load transmission to the structure's lower layers.

Considering the trade-off among elastic modulus, SEA, and practicality, the optimal dimensions for the NBCC lattice metamaterial are determined to be $s = 5$ mm and $D = 1.8$ mm, achieving an effective elastic modulus of 4.18 MPa and SEA of 57.6 Nm/kg, which represents a balanced compromise between compressive performance and energy absorption capability. This comprehensive analysis provides valuable insights into the design and optimization of NBCC lattice metamaterials for various engineering applications, highlighting the significance of carefully selecting geometric parameters to achieve the desired mechanical properties. The findings of this study contribute to the advancement of lattice metamaterial design and lay the foundation for further research and development of high-performance, lightweight structural components with enhanced load-bearing and energy absorption capabilities.

CRediT authorship contribution statement

Xuehao Song: Writing – review & editing, Writing – original draft, Software, Methodology, Investigation. **Chengjun Zeng:** Writing – review & editing, Writing – original draft, Funding acquisition, Data curation. **Junqi Hu:** Methodology, Visualization, Writing – review & editing. **Wei Zhao:** Writing – review & editing, Resources, Funding acquisition. **Liwu Liu:** Writing – review & editing, Validation, Formal analysis. **Yanju Liu:** Writing – review & editing, Supervision, Project administration, Conceptualization. **Jinsong Leng:** Writing – review & editing, Supervision, Funding acquisition.

Declaration of competing interest

The authors declare that they have no known competing financial interests or personal relationships that could have appeared to influence the work reported in this paper.

Acknowledgements

Appendix A. Supplementary material

Supplementary data to this article can be found online at https://doi.org/10.1016/j.compstruct.2025.119230.

Data availability

Data will be made available on request.

References

[1] Farzaneh A, Pawar N, Portela CM, Hopkins JB. Sequential metamaterials with alternating Poisson's ratios. Nat Commun 2022;13:1041.
[2] Nian Y, Wan S, Avcar M, Wang X, Hong R, Yue R, et al. Nature-inspired 3D printing-based double-graded aerospace negative Poisson's ratio metastructure: design, Fabrication, Investigation, optimization. Compos Struct 2024;348:118482.
[3] Du L, Shi W, Gao H, Jia H, Zhang Q, Liu M, et al. Mechanically programmable composite metamaterials with switchable positive/negative Poisson's ratio. Adv Funct Mater 2024;34:2314123.
[4] Choi J-C, Jeong HY, Sun J-H, Byun J, Oh J, Hwang SJ, et al. Bidirectional zero poisson's ratio elastomers with self-deformable soft mechanical metamaterials for stretchable displays. Adv Funct Mater 2024;2406725.
[5] Tan X, Li Y, Wang L, Yao K, Ji Q, Wang B, et al. Bioinspired Flexible and Programmable Negative Stiffness Mechanical Metamaterials. Adv Intell Syst 2023;5:2200400.
[6] Liu Y, Wang Y, Ren H, Meng Z, Chen X, Li Z, et al. Ultrastiff metamaterials generated through a multilayer strategy and topology optimization. Nat Commun 2024;15:2984.
[7] Meng Z, Liu M, Zhang Y, Chen CQ. Multi-step deformation mechanical metamaterials. J Mech Phys Solids 2020;144:104095.
[8] Noronha J, Dash J, Rogers J, Leary M, Brandt M, Qian M. Titanium multi-topology metamaterials with exceptional strength. Adv Mater 2024;36:2308715.
[9] Zhang Q, Guo D, Hu G. Tailored mechanical metamaterials with programmable quasi-zero-stiffness features for full-band vibration isolation. Adv Funct Mater 2021;31:2101428.
[10] Yue O, Wang X, Zhou Y, Bai Z, Zou X, Xie L, et al. Auxetic structure-assisted triboelectric nanogenerators for efficient energy collection and wearable sensing. Adv Energy Mater 2024;14:2400212.
[11] Viet NV, Zaki W. On exploration of directional extreme mechanical attributes and energy absorption of bending-dominated and buckling-induced negative Poisson's ratio metamaterials. Compos Struct 2024;349:118460.
[12] Zhang P, Qi D, Xue R, Liu K, Wu W, Li Y. Mechanical design and energy absorption performances of rational gradient lattice metamaterials. Compos Struct 2021;277:114606.
[13] Li B, Xin X, Lin C, Liu L, Liu Y, Leng J. Compressive properties and energy absorption of 4D printed auxetic mechanical metamaterials. Compos Struct 2024;340:118135.
[14] Fu K, Zhao Z, Jin L. Programmable granular metamaterials for reusable energy absorption. Adv Funct Mater 2019;29:1901258.
[15] Tang A, Yang Q, Liu J. Self-contacting metamaterials achieving asymmetric, non-reciprocal, and adjustable Poisson's ratios that break thermodynamic limits. Compos Struct 2024;348:118486.
[16] Jiang T, Han S, Han Q, Li C. Design and optimization of the dual-functional lattice-origami metamaterials. Compos Struct 2024;327:117670.
[17] Leanza S, Wu S, Sun X, Qi HJ, Zhao RR. Active materials for functional origami. Adv Mater 2024;36:2302066.
[18] Li T, Li Y. 3D Tiled auxetic metamaterial: a new family of mechanical metamaterial with high resilience and mechanical hysteresis. Adv Mater 2024;36:2309604.
[19] Chen Z, Lin Y-T, Salehi H, Che Z, Zhu Y, Ding J, et al. Advanced fabrication of mechanical metamaterials based on micro/nanoscale technology. Adv Eng Mater 2023;25:2300750.
[20] Chen X, Moughames J, Ji Q, Martínez JAI, Tan H, Ulliac G, et al. 3D lightweight mechanical metamaterial with nearly isotropic inelastic large deformation response. J Mech Phys Solids 2022;169:105057.
[21] Hamzehei R, Bodaghi M, Iglesias Martinez JA, Ji Q, Ulliac G, Kadic M, et al. Parrot beak-inspired metamaterials with friction and interlocking mechanisms 3D/4D printed in micro and macro scales for supreme energy absorption/dissipation. Adv Eng Mater 2023;25:2201842.
[22] Zeng C, Liu L, Hu Y, Zhao W, Xin X, Liu Y, et al. Stair-stepping mechanical metamaterials with programmable load plateaus. Adv Funct Mater 2024:2408887.
[23] Zhang F, Wen N, Wang L, Bai Y, Leng J. Design of 4D printed shape-changing tracheal stent and remote controlling actuation. Int J Smart Nano Mater 2021;12:375–89.
[24] Jiao P. Mechanical energy metamaterials in interstellar travel. Prog Mater Sci 2023;137:101132.
[25] Brooks AK, Chakravarty S, Ali M, Yadavalli VK. Kirigami-inspired biodesign for applications in healthcare. Adv Mater 2022;34:e2109550.
[26] Zhang Q, Dong J, Zhao Y, Zheng Y. Three-dimensional meta-architecture with programmable mechanical properties. Int J Smart Nano Mater 2022;13:152–65.
[27] Zeng C, Liu L, Lin C, Xin X, Liu Y, Leng J. 4D printed continuous fiber reinforced shape memory polymer composites with enhanced mechanical properties and shape memory effects. Compos A Appl Sci Manuf 2024;180:108085.
[28] Jiao P, Mueller J, Raney JR, Zheng X, Alavi AH. Mechanical metamaterials and beyond. Nat Commun 2023;14:6004.
[29] Wang D, Dong L, Gu G. 3D printed fractal metamaterials with tunable mechanical properties and shape reconfiguration. Adv Funct Mater 2023;33:2208849.
[30] Wang X, Li Z, Deng J, Gao T, Zeng K, Guo X, et al. Unprecedented strength enhancement observed in interpenetrating phase composites of aperiodic lattice metamaterials. Adv Funct Mater 2024:2406890.
[31] Montanari M, Brighenti R, Spagnoli A. Defect sensitivity mitigation in the compressive mechanical response of two-phase lattice metamaterials. Compos Struct 2023;323:117501.
[32] Li M, Chen H, Ma J, Chen Y. An origami metamaterial with distinct mechanical properties in three orthotropic directions. Int J Mech Sci 2024;283:109713.
[33] Zhang D, Li M, Qiu N, Yang J, Wu C, Steven G, et al. 4D-printed reusable metamaterial via shape memory effect for energy dissipation. Int J Mech Sci 2024;275:109309.
[34] Wang P, Yang F, Zheng B, Li P, Wang R, Li Y, et al. Breaking the Tradeoffs between Different Mechanical Properties in Bioinspired Hierarchical Lattice Metamaterials. Adv Funct Mater 2023;33:2305978.
[35] Rossi N, Romero I, Huespe AE. On the limit behavior of lattice-type metamaterials with bi-stable mechanisms. Int J Mech Sci 2024;276:109375.
[36] Gao J, Cao X, Xiao M, Yang Z, Zhou X, Li Y, et al. Rational designs of mechanical metamaterials: formulations, architectures, tessellations and prospects. Mater Sci Eng R Rep 2023;156:100755.
[37] Bauer J, Meza LR, Schaedler TA, Schwaiger R, Zheng X, Valdevit L. Nanolattices: an emerging class of mechanical metamaterials. Adv Mater 2017;29:1701850.
[38] Nian Y, Wan S, Avcar M, Yue R, Li M. 3D printing functionally graded metamaterial structure: design, fabrication, reinforcement, optimization. Int J Mech Sci 2023;258:108580.
[39] Zhou X, Ren L, Song Z, Li G, Zhang J, Li B, et al. Advances in 3D/4D printing of mechanical metamaterials: From manufacturing to applications. Compos B Eng 2023;254:110585.
[40] Zheng L, Karapiperis K, Kumar S, Kochmann DM. Unifying the design space and optimizing linear and nonlinear truss metamaterials by generative modeling. Nat Commun 2023;14:7563.

[41] Logakannan KP, Ramachandran V, Rengaswamy J, Gao Z, Ruan D. Quasi-static and dynamic compression behaviors of a novel auxetic structure. Compos Struct 2020; 254:112853.

[42] Nian Y, Wan S, Wang X, Zhou P, Avcar M, Li M. Study on crashworthiness of nature-inspired functionally graded lattice metamaterials for bridge pier protection against ship collision. Eng Struct 2023;277:115404.

[43] Hutchinson JR. Shear Coefficients for Timoshenko Beam Theory. J Appl Mech 2000;68:87–92.

[44] Li T, Sun J, Leng J, Liu Y. Quasi-static compressive behavior and energy absorption of novel cellular structures with varying cross-section dimension. Compos Struct 2023;306:116582.